Femtosecond time-resolved and two-dimensional vibrational sum frequency spectroscopic instrumentation to study structural dynamics at interfaces

Avishek Ghosh,[1,2] Marc Smits,[1,a)] Jens Bredenbeck,[1,b)] Niels Dijkhuizen,[1] and Mischa Bonn[1,2,c)]
[1]*FOM, Institute for Atomic and Molecular Physics (AMOLF), Kruislaan 407, 1098 SJ Amsterdam, The Netherlands*
[2]*Leiden Institute of Chemistry, Leiden University, P.O. Box 950, 2300 RA Leiden, The Netherlands*

(Received 9 June 2008; accepted 24 August 2008; published online 22 September 2008)

We present a novel setup to elucidate the dynamics of interfacial molecules specifically, using surface-selective femtosecond vibrational spectroscopy. The approach relies on a fourth-order nonlinear optical interaction at the interface. In the experiments, interfacial molecules are vibrationally excited by an intense, tunable femtosecond midinfrared (2500–3800 cm^{-1}) pump pulse, resonant with the molecular vibrations. The effect of the excitation and the subsequent relaxation to the equilibrium state are probed using broadband infrared+visible sum frequency generation (SFG) light, which provides the transient vibrational spectrum of interfacial molecules specifically. This IR pump-SFG probe setup has the ability to measure both vibrational population lifetimes as well as the vibrational coupling between different chemical moieties at interfaces. Vibrational lifetimes of interfacial molecules are determined in one-dimensional pump-SFG probe experiments, in which the response is monitored as a function of the delay between the pump and probe pulses. Vibrational coupling between molecular groups is determined in two-dimensional pump-SFG probe experiments, which monitor the response as a function of pump and probe frequencies at a fixed delay time. To allow for one setup to perform these multifaceted experiments, we have implemented several instrumentation techniques described here. The detection of the spectrally resolved differential SFG signal using a combination of a charge-coupled device camera and a piezocontrolled optical scanner, computer-controlled Fabry–Pérot etalons to shape and scan the IR pump pulse and the automated sample dispenser and sample trough height corrector are some of the novelties in this setup. © *2008 American Institute of Physics.* [DOI: 10.1063/1.2982058]

I. INTRODUCTION

Molecular interactions at interfaces play a crucial role in a diversity of chemical, biological, and physical processes present in our everyday macroscopic world. This makes a detailed understanding of interfacial molecular properties very important; interfacial properties are known to be significantly different from the bulk of the material itself. It has been a challenge to elucidate these interface-specific interactions owing to the technical difficulties in observing and monitoring selectively the response of the few monolayers of material that define the surface or the interface. The use of techniques such as atomic force microscopy,[1,2] scanning tunneling microscopy,[2–4] transmission electron microscopy,[5,6] low energy electron diffraction,[7,8] neutron reflectometry,[9] neutron scattering,[10] and x-ray diffraction studies[11,12] have greatly improved our understanding of the nature of surfaces and interfaces.[13] However, the applicability of these techniques is largely restricted to samples in ultrahigh vacuum conditions. Moreover, these techniques are not fully noninvasive and generally set specific requirements on the samples. Probing surfaces by optical techniques is, in general, more flexible and noninvasive; however existing techniques such as surface plasmon resonance[14,15] and reflection absorption IR spectroscopy[16–18] still lack surface or molecular specificity. In the recent past, the second order nonlinear optical techniques of second harmonic generation (SHG) and sum frequency generation[19–23] (SFG) have proven to be a versatile noninvasive tool for probing interfaces with excellent molecular and surface specificities. In the electric dipole approximation, even-ordered nonlinear optical processes such as SHG and SFG are forbidden in media with inversion symmetry. At surfaces and interfaces, the inversion symmetry of the medium is intrinsically broken, thus making SHG and SFG allowed optical processes. This very phenomenon makes these processes highly surface specific with submonolayer sensitivities at the interface of centrosymmetric media. These techniques are further appealing to the surface science community for the relative simplicity in implementation of a basic SHG or SFG probe setup.

Although an exhaustive list of literature is available on

a)Present address: MAPPER Lithography B.V., Computerlaan 15, 2628 XK Delft, The Netherlands.
b)Present address: Cluster of Excellence Macromolecular Complexes, Johann Wolfgang Goethe-University, Institute of Biophysics, Max-von-Laue-Strasse-1, 60438 Frankfurt/Main, Germany.
c)Author to whom correspondence should be addressed. Electronic mail: bonn@amolf.nl.

the theory of second order nonlinear processes,[24] briefly, the generation of second harmonic or sum frequency of the probing incident beams, is a function of the second order susceptibility tensor $\chi^{(2)}$ of the material and the incident electric field strengths, i.e.,

$$I_{SF} = L|\chi^{(2)}(\omega_{SF};\omega_1,\omega_2)|^2 I_1 I_2, \tag{1}$$

where L is the nonlinear Fresnel coefficient of the medium and I_1 and I_2 are the incident field intensities with frequencies ω_1 and ω_2, respectively. When $\omega_1=\omega_2$, the nonlinear optical process is called SHG and otherwise its SFG. The nonlinear susceptibility of a molecule $\chi^{(2)}$ is essentially a vector sum of all the molecular hyperpolarizabilities $\beta_n^{(2)}$ associated with every vibrational mode n in the molecule, averaged over all possible orientations:

$$\chi^{(2)} = \sum_n N_n \langle \beta_n^{(2)} \rangle, \tag{2}$$

where N_i is the number density of molecules. In centrosymmetric media, the net value of $\chi^{(2)}$ is zero and no generation of second harmonic or sum frequency response is observed. However, the net value of $\chi^{(2)}$ is finite in noncentrosymmetric media and at interfaces, which makes SHG/SFG a highly selective optical probe for surfaces.

With the development of broadband mid-IR pulses,[25] frequency-resolved vibrational SFG spectroscopy (VSFG) has received much attention in the recent past, for its ability to measure the vibrational spectrum of molecules at the interface with submonolayer sensitivity.[26] In VSFG, an infrared (IR) light pulse and a visible light pulse are overlapped at the interface to produce the SFG light. For VSFG, the nonlinear susceptibility can be expressed as a function of the IR frequency

$$\chi^{(2)} = A_{NR} e^{i\phi_{NR}} + \sum_n \frac{A_n (N_{0,n} - N_{1,n})}{\omega_{IR} - \omega_n + \iota\Gamma_n}. \tag{3}$$

Here the nonlinear susceptibility $\chi^{(2)}$, and hence the SFG signal, is enhanced when the IR frequency is resonant with a vibrational mode, as seen in the second term of Eq. (3). The amplitude of the resonant SFG signal is given by A_n, which is a function of the population difference between the ground and first excited vibrational states, $\Delta N_n = N_{0,n} - N_{1,n}$, ω_{IR} is the frequency of the incident IR pulse, ω_n is the vibrational resonance frequency, and Γ_n is the linewidth of the resonance. Generally, there may also be a nonresonant contribution to the overall SFG signal, characterized by amplitude A_{NR} and phase φ_{NR}. Although the nonresonant signal can exceed the resonant signal for, e.g., metallic substrates, for the interfaces studies here, the nonresonant contribution is generally small.

In the past two decades, much work in frequency- and polarization-resolved SFG has been devoted to characterizing and understanding various solid-gas, liquid-gas, and liquid-liquid interfaces.[27–46] Despite the apparent impact of this technique by providing the surface vibrational spectrum, static SFG spectroscopy falls short of providing direct information on the dynamics of molecular structures and intra-/intermolecular vibrational coupling, which evolve at ultrafast time scales. However, IR pump probe[47,48] and 2D-IR (Refs. 49 and 50) techniques developed in the recent past, have shown their advantage over static spectroscopy in their ability to directly probe the ultrafast molecular dynamics and vibrational coupling in bulk systems. Although the first literature on pump-probe SFG experiments using picosecond pulses to probe vibrational lifetimes of adsorbates on semiconductor[51] and on metal surfaces[52] appeared in the 1990s, the time and frequency resolutions and the applicability of the technique to any interface were restricted to picosecond molecular dynamics. With the development of short amplified pulses ($\leq$100 fs) and better detection techniques, broadband IR pump-probe SFG experiments with subpicosecond time resolution have now become a possibility. As a result, subpicosecond surface vibrational dynamics can be interrogated directly. In the recent past, pump-probe SFG experiments have been performed to study the mechanisms of adsorption and desorption of gases on catalytic metals under UHV conditions.[53–55] Recently time-resolved electronic SFG studies have interrogated probe molecules in hidden interfaces.[56] In this paper, we demonstrate a novel time-resolved SFG (TRSFG) setup that combines static broadband SFG spectroscopy with IR pump-probe and two-dimensional vibrational infrared spectroscopy (2D-IR) techniques to monitor ultrafast structural dynamics and coupling of molecules primarily at liquid-liquid and model biological interfaces, under normal laboratory conditions.

The basic principle of TRSFG is schematically shown in Figs. 1(a)–1(c) and that of 2D-IR spectroscopy in Figs. 1(d) and 1(e). In a pump-probe SFG experiment [experiment scheme shown in Fig. 1(a), energy-level diagram shown in Fig. 1(b)], the pump IR pulse excites molecules from the ground vibrational state ($v=0$) to the first excited state ($v=1$) in a two-step process: the high intensity IR pump pulse first prepares the two-level system by creating a vibrational coherence between the $v=0$ and $v=1$ state and then population is transferred from $v=0$ to $v=1$ state. If the anharmonicity of the vibration is sufficiently large, the excited state SFG signal ($v=1$ to $v=2$) is shifted out of the frequency window. Moreover, this signal will be very small, given the fact that the SFG intensity depends on the square of the surface population density.

This pump-induced population transfer from $v=0$ to $v=1$, transiently reduces the effective $\chi^{(2)}$ of the system since $\chi^{(2)} \sim \Delta N$. This perturbation in the equilibrium population distribution is observed as a *bleach* in the SFG probe signal, as schematically shown in Fig. 1(c). As the molecules relax back to the vibrational ground state, the equilibrium population distribution is regained: the SFG signal returns to its original magnitude as a function of the delay time between the IR pump pulse and SFG probe pulse pair. In this mode, TRSFG is fully analogous to the more widely applied transient IR absorption spectroscopy, except for the fact that the latter involves detection of a third-order coherence (two interactions with the pump IR field and one with the probe IR field), while the former involves the upconversion of the third-order coherence created by the pump and probe IR fields, to a fourth-order coherence by the visible pulse. Hence the TRSFG technique involves a $\chi^{(4)}$ optical interaction while static SFG spectroscopy is a $\chi^{(2)}$ process. The time

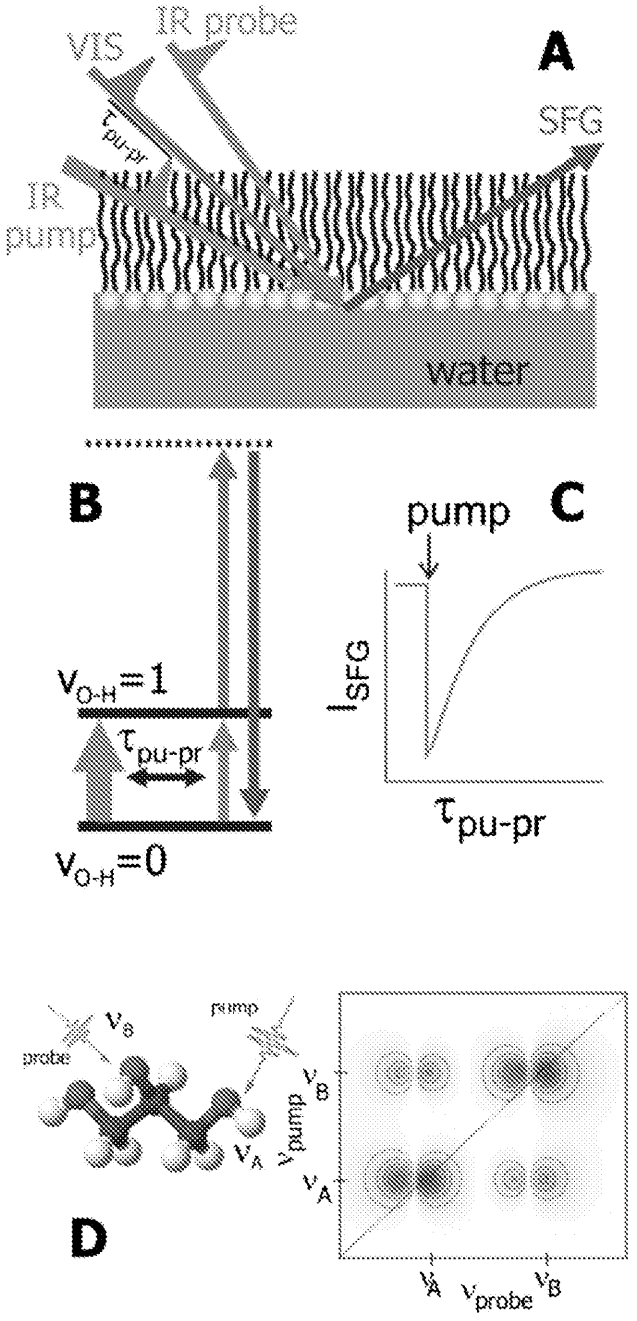

FIG. 1. (Color online) (a) Schematic representation of broadband pump-probe SFG spectroscopy of interfacial water at the water-lipid interface. The scheme represents the broadband probe IR pulse convoluted with a narrow band visible pulse to generate the vibrational SFG spectrum of water. The time delay τ represents the delay between the pump pulse and the probe pair. By scanning the delay and monitoring the modulation in the SFG signal, one can probe the femtosecond vibrational dynamics of interfacial molecules. (b) Energy level representation of the pump-probe SFG process. (c) Cartoon of the dynamics SFG transient showing the modulation of the SFG signal as a function of the pump-probe delay. (d) Cartoon representing the 2D-IR concept; the pump pulse excites ν_A vibrational mode and the probe pulse interrogates the ν_B mode in order to address the vibrational coupling between these modes. Also shown is a model 2D-IR plot. The one-color IR pump-probe response lies on the diagonal (dotted line) whereas the two-color coupling response is shown at the off-diagonals. The blue response is the bleach signal corresponding to the population excitation from $v=0$ to $v=1$ whereas the red response is the transient absorption of population from $v=1$ to $v=2$. The redshift of the $1\rightarrow 2$ response with respect to the $0\rightarrow 1$ response corresponds to the anharmonicity of the system.

dependence of the fourth-order signal is contained in the population densities of the ground (N_0) and the excited state (N_1), such that, in the absence of intermediate states:

$$I_{SFG} \propto [N_0(t) - N_1(t)]^2 = [1 - 2N_1(t)]^2 = [1 - 4N_1(t) + 4N_1^2(t)] \approx 1 - 4N_1(t). \quad (4)$$

The observed bleach of the signal is proportional to the square of the population difference, rather than simply the difference. This has some interesting consequences: for example, when the pump excites 10% of the ground state molecules to the excited state at zero pump-probe delay, the population difference amounts to $\Delta N=0.9-0.1=0.8$. The signal level thus decreases to $(\Delta N)^2=0.64$ and a bleach of 36% is observed. We further note that, for sufficiently small N_1, the signal will decay with T_1.

This setup also supports a novel 2D-SFG technique—the surface-specific analog of the widely known 2D-IR. The basic idea behind 2D-IR is to transpose the elegant methods originally developed in multidimensional NMR[57] to study coupling of nuclear spins, to coupling of vibrational transitions. In a 2D-IR experiment [see Fig. 1(d)], one specific vibrational mode A with frequency ν_A is excited, i.e., pumped, and the effect of this excitation is probed at ν_A, and also at the frequency ν_B of a different mode B. If the modes are completely uncoupled, any effect of exciting mode A on mode B will be absent, and a spectral response will only be observed for identical pump and probe frequencies. As plotted schematically in Fig. 1(d), the IR absorption response as a function of the pump and probe frequencies will give rise to diagonal peaks. If, in addition, the two modes are coupled so-called cross peaks will appear on the off-diagonal. In complete analogy to NMR, strength of the cross peak is determined by the degree of coupling, which is related to the distances and orientations between the coupled vibrators and hence the relative molecular structures.[58] As such, the 2D-IR spectrum contains detailed information on the biomolecular structure and conformational fluctuations.[59–64] The principle idea of 2D-IR spectroscopy has now been extended to probe molecular vibrational coupling of molecules at the interface, using the recently developed 2D SFG (2D-SFG) technique.[65] Here, individual modes are excited using a narrow band pump IR pulse and the SFG spectrum due to the broadband probe IR is recorded at every pump frequency. Plotting the intensities of the pump-probe SFG as a function of pump and probe IR frequencies at a certain delay, will give rise to one-color pump-probe SFG bleach signals on the diagonal and two-color pump-probe SFG cross peaks on the off-diagonal, indicative of vibrational coupling.

In this paper, we shall present the instrumentation for the novel pump-probe SFG setup. The merit of the approach will be illustrated by recently obtained results at the water-air[66] and water-lipid[67] interfaces. With this instrumentation, we have also successfully demonstrated the first 2D-SFG experiment on a monolayer of dodecanol on water.[65] The state-of-the-art instrumentation includes generation of high intensity mid-IR pulses (tunable in 2800–3500 cm^{-1}), shaping the pump IR bandwidth using a computer-controlled Fabry–Pérot interferometer, a feedback-controlled trough height

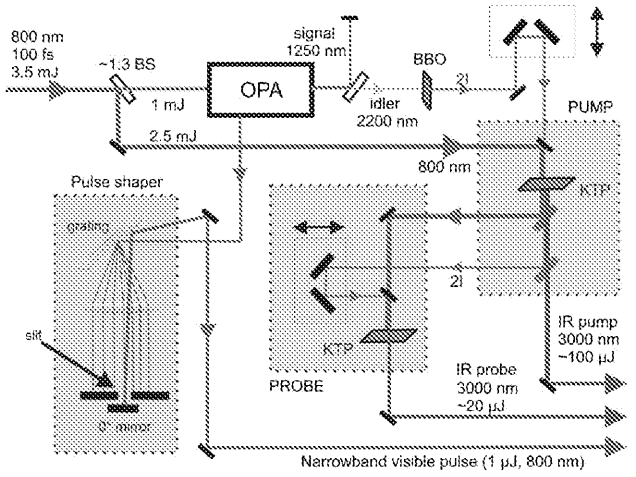

FIG. 2. (Color online) Scheme for generation of pump and probe IR by difference frequency mixing of amplified 800 nm and doubled idler pulse. The difference frequency mixing in the KTP crystals are a type-II process, with the polarizations of the 800 nm, doubled idler, and the IR pulse being horizontal, vertical, and horizontal, respectively. The home-built pulse shaper disperses the 800 nm beam and the frequency components are imaged by the lens onto the Fourier plane where a mirror and a slit are placed. The slit is adjusted to select a narrow band frequency and the 0° mirror behind the slit causes the selected frequency to retrace the path, back onto the grating and is coupled out.

corrector for evaporation of sample and a feedback-controlled sample injector to add fresh sample during an experiment, detection of the spectrally resolved IR pump-SFG probe dynamics signal using a combination of an intensified charge-coupled device (ICCD) array and a 500 Hz piezocontrolled optical scanner. Software was written in LABVIEW to control the hardware and the data acquisition.

II. EXPERIMENTAL

A. Generation of mid-IR and upconversion pulses

A conventional broadband SFG setup[45] typically requires a pair of probe laser pulses, i.e., the weak broadband IR [~10 μJ, full width at half maximum (FWHM) ~150 cm^{-1}] and the narrow band visible upconversion pulse (~1 μJ, FWHM <10 cm^{-1}), to generate SFG at the surface. However, for the TRSFG experiments, an additional high intensity (~40 μJ) mid-IR pump pulse is required to excite ground state molecules to a higher vibrational state. In this section, we shall present a scheme to generate high (pump) and low (probe) intensity mid-IR pulses and a homebuilt pulse shaper for generating the narrow band visible upconversion pulse.

The laser system consists of a Verdi-pumped ($Nd:YVO_4$) oscillator (Mira 900, Coherent) to generate 800 nm pulses with sub-100-fs pulse duration. This provides the seed pulses for a regenerative multipass amplifier (Titan, Quantronix), that is pumped by a high energy Nd:YLF (yttrium lithium fluoride) laser (DQ-527, Quantronix). The multipass amplifier produces ~3.5 mJ/pulse centered at 800 nm with a bandwidth of ~12 nm with repetition rate of 1 kHz and ~100 fs pulse duration. The pump and probe IR generation scheme[68] is shown in Fig. 2. A commercial optical parametric amplifier (TOPAS, Light Conversion) is pumped by 30% (1 mJ) of the amplified near-IR (NIR) (~800 nm) beam to generate 330 μJ of tunable signal (~1250 nm) and idler (~2200 nm) beams. The idler is doubled in a type-I β-barium borate crystal (BBO) ($5\times5\times3$ mm^3, $\phi=90°$, $\theta=22.2°$) to generate ~45 μJ of ~1100 nm pulses. Difference frequency mixing (DFM) of the doubled idler beam with the remaining 70% (2.5 mJ) of the amplified NIR beam in a type-II $KTiOPO_4$ (potassium titanyl phosphate) crystal ($10\times10\times3$ mm^3, $\phi=0°$, $\theta=41.8°$) produces ~100 μJ mid-IR pulses (~3000 nm). Frequency tuning of the mid-IR pulse requires changing the fundamental idler frequency at the OPA and subsequently optimizing the phase matching angles of the idler doubling crystal (BBO) and the DFM crystal (KTP). Using this approach of DFM, the center frequency of the generated high intensity mid-IR pulses is limited by the tuning curves of the KTP and the BBO crystals corresponding to the doubled idler and the NIR frequencies; generated mid-IR frequencies range from 2860 nm (3496 cm^{-1}) to 3570 nm (2801 cm^{-1}), with pulse energies in the order of 80–100 μJ. Typical FWHM bandwidths of the mid-IR pulse ~200 cm^{-1}. This is used as the IR pump pulse; the intensity is typically attenuated using a neutral density filter to ~40 μJ to prevent cumulative heating of the interface which may affect the lipid phase and cause irreversible chemical changes in some of the lipid samples. The residual NIR 800 nm pulse and the amplified doubled idler pulse after the pump IR generation, are mixed in a second type-II KTP crystal ($5\times5\times3$ mm^3, $\phi=0°$, $\theta=41.8°$), to generate ~25 μJ of probe IR (FWHM ~150 cm^{-1}). In this manner, the probe IR wavelength can be tuned independently of the pump IR wavelength to a limited extent—the pump and the probe IR frequencies can be detuned by 200 cm^{-1}. As such, two-color pump-probe SFG experiments[69] without using a second OPA are possible. The limited detuning is caused by the fact that the doubled idler frequency which is used for IR pump generation is also used to generate the probe IR frequency. Hence the phase matching angle of the KTP crystal in the probe path, cannot be very different from that of the KTP crystal in the pump path.

Also shown in Fig. 2, is a homebuilt pulse shaper, which is used to reduce the bandwidth of the visible upconversion pulse, to maintain high frequency resolution of the SFG spectrum. The input of the pulse shaper is the residual NIR (FWHM ~12 nm) after pumping the OPA. The grating in the homebuilt pulse shaper disperses this NIR pulse (Fourier decomposition of pulse from time to frequency domain) and the frequency components are spatially separated by the lens onto the Fourier plane where a mirror and a slit are placed. The slit is adjusted to spatially select a narrow band frequency and the 0° mirror behind the slit causes the selected frequency to retrace the path, back onto the grating and is coupled out (Fourier recomposition of pulse from frequency to time domain). The output of the pulse shaper is typically a narrow band (FWHM ~0.6 nm, 10 cm^{-1}) visible pulse.

The 2D-SFG instrumentation involves placing a piezo-controlled Fabry–Pérot etalon (Thor Laboratories) in the pump IR path of the existing TRSFG scheme (see Fig. 3). By adjusting the voltage on the piezoelectric actuators, one can

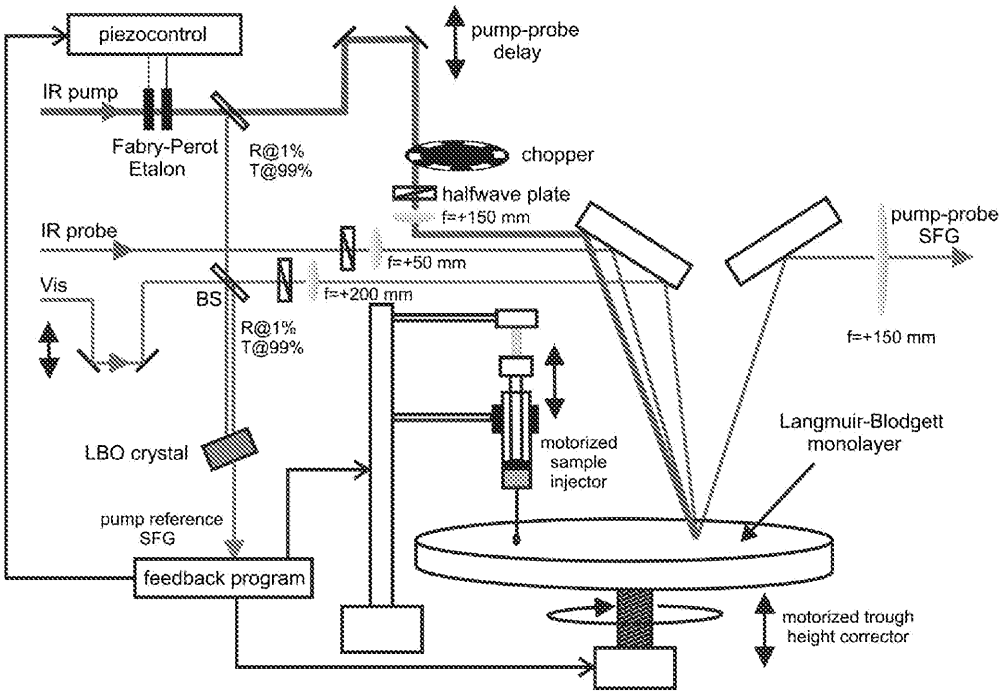

FIG. 3. (Color online) Instrumentation at sample (see text for details).

control the parallelism and the distance between the mirrors of the etalon, thus controlling the center frequency and width of the pulse. The etalon shapes the broadband pump IR pulse (FWHM ~ 200 cm^{-1}) into a narrow band pulse (FWHM ~ 20 cm^{-1}). Typical energies of the shaped pump IR pulses is ~ 10 μJ, due to inherent losses in the Fabry–Pérot etalon. As shown in Fig. 3, a small part (1%) of the pump IR and the visible upconversion pulse are mixed in a lithium niobate crystal ($LiNbO_3$) to generate a sum frequency signal which is used to calibrate the excitation frequency.

B. Instrumentation at sample

In Fig. 3, the schematic for the instrumentation at the sample is shown. The pump IR, probe IR, and the visible beams are kept in the same vertical plane of incidence and focused down to 150, 100, and 100 μm, respectively. The beams are overlapped at the sample interface, making incidence angles of 56°, 46°, and 50° with respect to the surface normal. The probe IR and the visible beam generate the SFG spectrum at the interface when the two incident fields are temporally and the spatially overlapped. The temporal overlap can be achieved by scanning the delay of the visible pulse. The spatial and temporal overlaps of the pump IR with the SFG probe pair can be optimized by monitoring the third-order nonlinear optical process of infrared-infrared-visible-SFG (IIV-SFG),[70] which occurs only when all the three incident fields overlap. The sample is held in a home-built Teflon™ trough (~ 5 cm radius) which is rotated at ~ 5 rpm to reduce cumulative heating. The sample is effectively refreshed every approximately five laser shots. This trough is supported on a motorized labjack, specially designed to damp mechanical vibrations while rotating the trough or while moving the trough vertically. To account for the evaporation of the water subphase, the vertical position of the SFG spectrum on the CCD chip is monitored by the measurement program throughout the experiment. Due to evaporation of the water subphase over long data acquisition times, the surface height changes and moves out of the foci of the incident beams. As a result, the SFG signal decreases in intensity and is displaced vertically on the CCD chip. The latter effect is used as a feedback to correct the trough height for evaporation, by a motorized (Standa stepper motor controller 8SMC1-USBh) labjack, to restore the signal (and intensity) at the original position on the CCD. Some of the experiments require hours of SFG signal acquisition. Over this period, the surface pressure of the lipid monolayer tends to drop, leading to a drop in signal intensity. One possible reason for this is that the Teflon™ trough becomes coated with lipids. The effect of the pressure drop can be circumvented by the addition of fresh surfactants onto the monolayer. We verified that the shape of the SFG spectra of a "repaired" monolayer was identical to that of a freshly prepared one. The monolayer repair during data acquisition was performed when the probe SFG signal intensity drops by 20% of the original SFG intensity at the start of the experiment. The computer-controlled feedback program uses a motorized lipid sample injector (syringe filled with the lipid solution in chloroform, attached to a Standa stepper motor) to add a few drops of the lipid solution onto the water subphase, and allowing the system to equilibrate. This automation of sample control allows us to perform many hours of scanning without human presence.

C. Detection and data acquisition

The pump-probe SFG signal generated from the interface is collected and collimated by a 150 mm positive lens

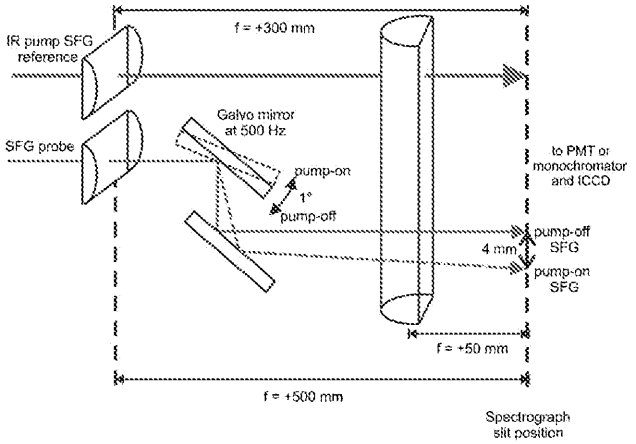

FIG. 4. (Color online) Scheme for the detection path, including the galvanometric scanning mirror to spatially separate the pump-on and pump-off SFG spectra. Cylindrical lenses are used to facilitate focusing of the pump reference SFG, pump-on and pump-off SFG beams onto the spectrometer slit. The lenses on the left focus on the vertical plane whereas the lens on the right, close to the spectrometer slit, focuses the pump reference SFG and collimates the pump-on and pump-off SFG beams onto the slit. The focal lengths of the two cylindrical lenses on the left are different since the SFG beam paths are different. The scanning mirror is used only when the data acquisition is in the spectral mode (CCD mode) and not in the photon-counting mode (PMT mode).

(see Fig. 4) and then sent to either a photomultiplier tube (PMT) (Acton Research, PD438) or a monochromator/ICCD camera (Princeton Instruments, PI-MAX2:512 Gen III), depending on the application. The PMT is used to record the spectrally integrated pump-probe SFG signal in the photon-counting mode.[66] The electronics used for the PMT detection is shown in Fig. 5 with green lines. The PMT signal is averaged on a boxcar integrator, with typical electronic gate widths of ~3 μs. The averaged PMT signal is then sent to the PC through an analog-to-digital coverter (ADC) (National Instruments, 16 bits). To separate the pump-on and pump-off SFG photons, a diode laser (continuous wave) is transmitted through the same hole in the chopper as the

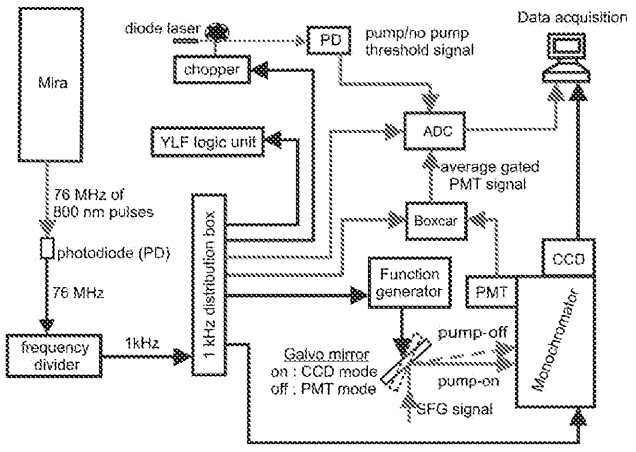

FIG. 5. (Color online) Scheme for the electronics in the setup. The green channels are in use only when experiments are done with the PMT. For the chopper output signal, a cheap diode laser is used and is aligned through the same hole as the pump IR beam and is detected by a PD. The signals from the PD and from the function generator are sent to an oscilloscope for tuning the phases.

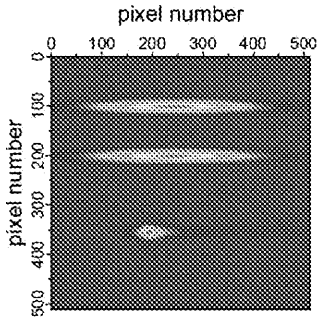

FIG. 6. (Color online) Image of the CCD camera, corrected for large spikes presumably caused by cosmic radiation. The upper and lower traces depict the broadband SFG signal with and without pump, respectively, and the lower trace shows the spectrum of the pump pulse.

pump beam and onto a photodiode (PD) as schematically shown in Fig. 5. The PD signal is sent to the PC via the ADC; this provides the information as to which laser shot corresponds to pump-on and which one to pump-off SFG signal.

For obtaining spectral information during a pump-probe SFG experiment, the SFG signal is dispersed by a monochromator (Acton SpectroPro300i) and the image is recorded on a CCD chip (512×512 pixels, 24 μm/pixel). In order to record the SFG spectra with and without the effect of the IR excitation, before sending the SFG signal to the monochromator, the pump-on and pump-off SFG signals are spatially separated using a galvanometric servocontrolled optical scanning mirror (GSI Lumonics, VM2000) synchronized with the 1 kHz laser repetition rate, following the scheme shown in Fig. 4. The galvanomirror is supplied with a 500 Hz sinusoid voltage from a function generator (Agilent Technologies, 20 MHz/arbitrary waveform generator), by which the mirror oscillates with an angle of ~1° about the mirror axis. This translates to a spatial separation of ~4 mm on the CCD chip (total chip size: 12 mm=512 pixels) between the pump-on and pump-off SFG signal. To ensure that the pumped shot always falls onto the same position on the chip, the phase of the scanning mirror is synchronized with the phase of the chopper output signal. By binning the individual pump-on and pump-off SFG spectra, vertically on the CCD chip, we can obtain the spectral information with and without the IR excitation. A typical screenshot (see Fig. 6) includes the pump-on SFG and the pump-off SFG images on the CCD chip with the galvanomirror in action, which spatially separates the two images. For the 2D-SFG experiments, the reference SFG [generated by mixing a small fraction of the narrow band visible and the narrow band pump beams in a LiB_3O_5 (lithium triborate) crystal] is sent to the monochromator and the CCD via the detection path shown in Fig. 4). The image of this reference SFG on the CCD chip can also be seen in Fig. 6; the computer program uses this image as a feedback for the piezocontroller of the Fabry–Pérot etalons to adjust the bandwidth and center frequency of the IR pump pulse.

D. Electronics

The electronics for this setup are shown schematically in Fig. 5. A small fraction of the 76 MHz 800 nm seed pulses

from the oscillator is detected by a fast PD. This PD signal is then divided by an electronic frequency divider to generate a 1 kHz signal which is used to trigger the Nd:YLF laser and all the electronics in the setup, including the phase-locked optical chopper, the boxcar integrator, the ADC, the function generator for the galvanomirror and the CCD camera.

E. Software

The data acquisition software was written in LABVIEW 8. Typical CCD readouts such as presented in Fig. 6 contain the spectrally dispersed pump-on, pump-off, and pump reference SFG signals. The software controls the pump-probe delay line and analyzes the CCD images in real time to establish whether specific action should be taken, such as trough height modification or adjustment of the Fabry–Pérot piezovoltage.

The ratio between the pump-on/pump-off spectra is instantaneously calculated to monitor in real time any spectral shifts during a pump-probe SFG experiment. The pump-probe delays for the TRSFG, the Fabry–Pérot voltages for the 2D-SFG, the spectrograph settings, and the function generator settings for the galvanic mirror can all be set in specific panels in the software. The spectrograph settings include the grating, the center wavelength of detection, the pixel-wavelength calibration, intensifier gain, and the signal acquisition times. A function generator is included to set phase, the amplitude of the oscillation and the offset position of the scanning galvanomirror. The number of scans, the sample height control, and the pump polarization (controlling the motorized half wave plate in the pump IR path) may also be adjusted in the software. The ratio between the integrated pump-on and pump-off SFG spectra is plotted as a function of pump-probe delay during the scan, for online monitoring purposes. The feedback to the sample control program is taken from the CCD image (Fig. 6) after every scan. The signals are fit to Lorentzians as a function of the vertical pixel position to reliably determine the vertical position of the spectra on the CCD camera. As soon as the spectrum is observed to have been shifted vertically by a preset number of pixels (typically 10), the feedback control program moves the trough height motors to reposition the signal. As discussed earlier, to account for sample degradation over long acquisition times, when the amplitude of the Lorentzian falls by ~30% of the original amplitude, the sample injector dispenses a precalibrated number of drops required to restore the original signal amplitude. This way the SFG signals are maintained at their initial conditions before every scan, throughout the experiment, typically consisting of 100 scans. A typical scan is performed from −1.8 to 100 ps, in linear steps of 50–500 fs and logarithmic thereafter.

III. RESULTS

A. Instrument response

The spatiotemporal overlap of the pump and probe beams and the instrument response were determined by scanning the delay of the pump IR with respect to the probe SFG pair and recording the IIV-SFG intensity.[70] Figure 7(a) shows the energy-level schematic for the IIV-SFG process, while Fig. 7(b) shows a typical pump-probe IIV-SFG cross-correlation trace at the 1,2 dimyristoyl Glycero-3-phospho-L-serine (DMPS)-water interface. The pump and probe IR are reasonably described as Fourier-limited pulses with typical widths of ~120 fs.

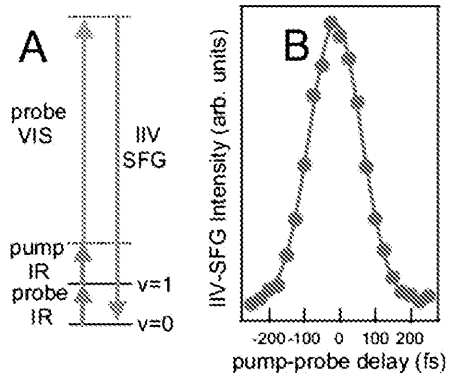

FIG. 7. (Color online) (a) Schematic for the third-order IIV-SFG process generated by overlapping the pump IR and the probe pulse pair at the interface. In this process, only the probe IR is resonant with the fundamental vibrational transition. By scanning the pump pulse in time with respect to the probe pair, one can obtain a cross-correlation trace (b) as a function of the pump-probe delay. The narrow band visible pulse is about 2–3 ps long, so the cross-correlation trace is determined by the temporal convolution of the two IR pulses. These results demonstrate that the typical time resolution of the TR-SFG experiment amounts to ~120 fs. The time resolution of the 2D-SFG experiment is longer (~1 ps) and asymmetric around time-zero (Gaussian rise and exponential decay) since the pump IR pulse is shaped to a narrow band by the Fabry–Pérot etalon.

B. TR-SFG experiments

Time-resolved SFG experiments were performed at the water-air and water-lipid interfaces. For both systems, ultrapure water was used (Millipore filtered, 18 MΩ resistivity) as the subphase supported in a home-built Teflon trough. For the water-lipid studies, the lipid used was DMPS (sodium salt) purchased from Avanti Polar Lipids. A solution of DMPS was prepared in 90% chloroform and 10% methanol (Sigma Aldrich) and a Langmuir monolayer film of lipid molecules was prepared by careful addition of drops of the lipid solution in steps of 0.5 μl on the water subphase while monitoring the surface pressure of the monolayer with a Wilhelmy-plate based tensiometer (model Kibron DeltaPi). The surface pressure was maintained such that all experiments were performed in the liquid condensed phase of the lipid monolayer.

In the time-resolved pump-probe SFG experiment, the vibrational lifetimes of the interfacial water molecules were determined by scanning the delay of the pump IR pulse in time with respect to the probe pair, while monitoring the modulation in the generated SFG spectrum. In order to generate a pump-on and pump-off SFG signal, the 1 kHz pump IR pulse is chopped to 500 Hz with a phase-locked optical chopper synchronized with the laser repetition rate. The effect of excitation on the SFG spectrum of the ground state molecules due to the pump IR pulse, is observed as a ratio between the "pump-on" and the "pump-off" signals at every pump-probe delay. This way, for every laser shot, a reference

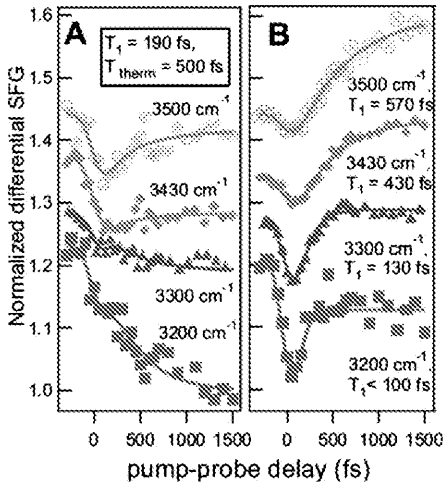

FIG. 8. (Color online) Time-resolved SFG trace. Figure 6(a) shows the vibrational dynamics of the neat water/interface;[66] (b) water/lipid interface.[67]

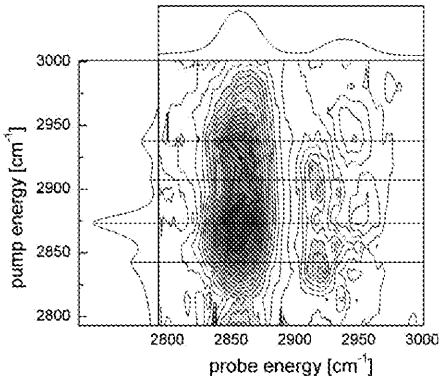

FIG. 9. (Color online) 2D pump-probe SFG plot of dodecanol on D_2O subphase.[65] The IR spectrum of dodecanol is shown in Fig. 8(a), which the narrow band pump IR interrogates through a frequency scan. The SFG spectrum of dodecanol due to the broadband probe IR is plotted in Fig. 8(b), which indicates only three SFG active modes. Figures 8(c) and 8(d) show a plot of the pump-probe signal as a function of the pump and probe IR frequencies, at *p*- and *s*-polarizations of the pump IR pulse, respectively.

pump-off SFG spectrum was recorded along with the pump-on SFG spectrum. At zero pump-probe delay, the excitation pulse depletes population from the equilibrium ground vibrational state to an excited vibrational state. This results in a bleach in the SFG signal intensity of the ground state. The recovery of the SFG signal as a function of the pump-probe delay time is a signature of the mechanism of vibrational relaxation of the excited state molecules back to the equilibrium ground state. We demonstrate this by performing the TRSFG experiments at fixed frequencies of the pump and probe IR pulses, resonant with the fundamental vibrational modes in hydrogen-bonded regime of the SFG spectrum of water. The typical TRSFG transients for the water-air and water-DMPS interfaces are shown in Figs. 8(a) and 8(b) respectively, with the normalized differential SFG signal plotted as a function of the pump-probe delay time. We observe that at the neat water-air interface, the relaxation dynamics of the excited water molecules are identical in different hydrogen bond environments and can be described by the model used to describe the dynamics in bulk water, which is dominated by an ultrafast Förster-type energy transfer between neighboring water molecules. This led us to conclude that the Förster-type energy transfer also dominates at the neat water-air interface and there is an ultrafast energy exchange between surface and bulk water molecules.[66] At the water-lipid interface, however, we found that the relaxation dynamics depend critically on the hydrogen bond environments being probed and no evidence for a fast Förster energy transfer was found. This led us to conclude that there is no significant communication between different hydrogen-bonded environments at the water-lipid interface[67] and water molecules interfacial with the lipid monolayer have a more heterogeneous environment than those at the neat water-air interface. These differences in water structure at different interfaces could not be elucidated by the static SFG spectra on these systems whereas clearly demonstrated by the TRSFG experiments.

C. 2D-SFG experiments

In our first 2D-SFG study, we investigated a dodecanol monolayer on water—a model system for biological membranes—in the region of the C–H stretching modes of the alkyl chains. The sample was prepared by placing a small crystal of 1-dodecanol (Sigma Aldrich) in contact with water (D_2O, to suppress interferences with the O–H stretch vibration of H_2O). In the 2D-SFG experiment, changes in the SFG probe spectra are recorded, at a certain pump-probe time delay, as the narrow band pump IR frequency is scanned across the bandwidth of the probe IR and thereby sequentially exciting all the IR-active CH_3 and CH_2 modes of the dodecanol molecules at the interface. Figure 9 shows the 2D-SFG spectra of the self-assembled dodecanol monolayer, at 0.7 ps pump-probe delay, at parallel [Fig. 9(c)] and perpendicular [Fig. 9(d)] polarizations of the pump IR pulse with respect to probe IR pulse. In addition to the diagonal peaks, several off-diagonal peaks appear (indicated by orange arrows) that indicate mode coupling. As SFG selection rules apply for the probe process, off-diagonal peaks reporting on vibrational coupling, appear at the two frequencies corresponding to the two peaks in the static SFG spectrum. We observe that in addition to the expected coupling between the CH_3(ss) and CH_3(as) modes (being two modes of the same functional group), there exists a remarkably strong coupling between the CH_2(as) and CH_3(ss) vibrational modes; suggesting a strong mechanical coupling between these otherwise weak transition dipole coupled C–H modes. Hence, with this novel 2D-SFG instrumentation we have thus successfully demonstrated the first surface implementation of an ultrafast 2D-IR spectroscopy technique.[65]

IV. CONCLUSION AND SCOPE

We have successfully developed and implemented novel instrumentation to perform time-resolved and 2D-SFG spectroscopy on interfacial molecules in a spectrally resolved manner. This instrumentation has allowed us to study the dynamics of water molecules at the neat water/air[66] and the

water/lipid[67] interfaces and also the dynamics of energy flow in biological model membranes.[69] This instrumentation has also allowed us to perform the first proof-of-principle 2D-SFG experiment to study the vibrational coupling between the symmetric and antisymmetric/Fermi resonance modes of the $-CH_3$ group in dodecanol at the dodecanol/D_2O interface.[65] The setup has recently been extended to study time-dependent polarization anisotropy at interfaces, by recording the SFG probe signal with different pump polarizations at different pump-probe delays.

ACKNOWLEDGMENTS

This work was part of the research program of the Stichting Fundamenteel Onderzoek der Materie (Foundation for Fundamental Research on Matter) with financial support from the Nederlandse Organisatie voor Wetenschappelijk Onderzoek (Netherlands Organization for the Advancement of Research). We are grateful to Kramer Campen for his help in preparing this manuscript.

[1] H. G. Hansma, Annu. Rev. Phys. Chem. **52**, 71 (2001).
[2] L. C. Giancarlo and G. W. Flynn, Annu. Rev. Phys. Chem. **49**, 297 (1998).
[3] D. M. Cyr, B. Venkataraman, and G. W. Flynn, Chem. Mater. **8**, 1600 (1996).
[4] R. J. Hamers, Annu. Rev. Phys. Chem. **40**, 531 (1989).
[5] W. Sigle, Annu. Rev. Mater. Res. **35**, 559 (2005).
[6] A. K. Petford-Long and A. N. Chiaramonti, Annu. Rev. Mater. Res. **38**, 559 (2008).
[7] M. A. Chesters and G. A. Somorjai, Annu. Rev. Mater. Sci. **5**, 99 (1975).
[8] F. Jona, J. Phys. C **11**, 4271 (1978).
[9] R. K. Thomas, Annu. Rev. Phys. Chem. **55**, 391 (2004).
[10] F. R. Trouw and D. L. Price, Annu. Rev. Phys. Chem. **50**, 571 (1999).
[11] M. L. Schlossman and A. M. Tikhonov, Annu. Rev. Phys. Chem. **59**, 153 (2008).
[12] J. Milhaud, Biochim. Biophys. Acta **1663**, 19 (2004).
[13] G. Somorjai, *Chemistry in Two Dimensions: Surfaces* (Cornell University Press, Ithaca, NY, 1981).
[14] S. L. McGurk, R. J. Green, G. H. W. Sanders, M. C. Davies, C. J. Roberts, S. J. B. Tendler, and P. M. Williams, Langmuir **15**, 5136 (1999).
[15] K. A. Willets and R. P. Van Duyne, Annu. Rev. Phys. Chem. **58**, 267 (2007).
[16] M. Trenary, Annu. Rev. Phys. Chem. **51**, 381 (2000).
[17] K. Itoh and H. Oguri, Langmuir **22**, 9208 (2006).
[18] I. Estrela-Lopis, G. Brezesinski, and H. Mohwald, Biophys. J. **80**, 749 (2001).
[19] Y. R. Shen, Annu. Rev. Phys. Chem. **40**, 327 (1989).
[20] Y. R. Shen, Nature (London) **337**, 519 (1989).
[21] T. F. Heinz and G. A. Reider, Trends Analyt. Chem. **8**, 235 (1989).
[22] K. B. Eisenthal, Chem. Rev. (Washington, D.C.) **96**, 1343 (1996).
[23] K. B. Eisenthal, Annu. Rev. Phys. Chem. **43**, 627 (1992).
[24] Y. R. Shen, *The Principles of Nonlinear Optics* (Wiley, New York, 1984).
[25] F. Seifert, V. Petrov, and M. Woerner, Opt. Lett. **19**, 2009 (1994).
[26] M. Buck and M. Himmelhaus, J. Vac. Sci. Technol. A **19**, 2717 (2001).
[27] J. C. Conboy, M. C. Messmer, and G. L. Richmond, J. Phys. Chem. **100**, 7617 (1996).
[28] G. L. Richmond, Annu. Rev. Phys. Chem. **52**, 357 (2001).
[29] Q. Du, R. Superfine, E. Freysz, and Y. R. Shen, Phys. Rev. Lett. **70**, 2313 (1993).
[30] L. F. Scatena, M. G. Brown, and G. L. Richmond, Science **292**, 908 (2001).
[31] M. R. Watry, T. L. Tarbuck, and G. L. Richmond, J. Phys. Chem. B **107**, 512 (2003).
[32] M. Bonn, C. Hess, and M. Wolf, J. Chem. Phys. **115**, 7725 (2001).
[33] D. E. Gragson, B. M. McCarty, and G. L. Richmond, J. Phys. Chem. **100**, 14272 (1996).
[34] R. A. Walker, D. E. Gragson, and G. L. Richmond, Colloids Surf., A **154**, 175 (1999).
[35] M. G. Brown, D. S. Walker, E. A. Raymond, and G. L. Richmond, J. Phys. Chem. B **107**, 237 (2003).
[36] A. J. Hopkins, C. L. McFearin, and G. L. Richmond, Curr. Opin. Solid State Mater. Sci. **9**, 19 (2005).
[37] X. L. Zhao, S. W. Ong, and K. B. Eisenthal, Chem. Phys. Lett. **202**, 513 (1993).
[38] D. Zhang, J. Gutow, and K. B. Eisenthal, J. Phys. Chem. **98**, 13729 (1994).
[39] J. Kim and P. S. Cremer, J. Am. Chem. Soc. **122**, 12371 (2000).
[40] R. Lu, W. Gan, B. H. Wu, H. Chen, and H. F. Wang, J. Phys. Chem. B **108**, 7297 (2004).
[41] E. Tyrode, C. M. Johnson, A. Kumpulainen, M. W. Rutland, and P. M. Claesson, J. Am. Chem. Soc. **127**, 16848 (2005).
[42] H. Chen, W. Gan, B. Wu, Z. Z. Wu, and H. Wang, Chem. Phys. Lett. **408**, 284 (2005).
[43] X. Y. Chen, M. L. Clarke, J. Wang, and Z. Chen, Int. J. Mod. Phys. B **19**, 691 (2005).
[44] J. Wang, X. Y. Chen, M. L. Clarke, and Z. Chen, Proc. Natl. Acad. Sci. U.S.A. **102**, 4978 (2005).
[45] S. Roke, J. Schins, M. Muller, and M. Bonn, Phys. Rev. Lett. **90**, 128101 (2003).
[46] M. Bonn, S. Roke, O. Berg, L. B. F. Juurlink, A. Stamouli, and M. Muller, J. Phys. Chem. B **108**, 19083 (2004).
[47] E. T. J. Nibbering, H. Fidder, and E. Pines, Annu. Rev. Phys. Chem. **56**, 337 (2005).
[48] J. C. Owrutsky, D. Raftery, and R. M. Hochstrasser, Annu. Rev. Phys. Chem. **45**, 519 (1994).
[49] D. M. Jonas, Annu. Rev. Phys. Chem. **54**, 425 (2003).
[50] P. Hamm, J. Helbing, and J. Bredenbeck, Annu. Rev. Phys. Chem. **59**, 291 (2008).
[51] P. Guyotsionnest, P. Dumas, Y. J. Chabal, and G. S. Higashi, Phys. Rev. Lett. **64**, 2156 (1990).
[52] A. L. Harris, L. Rothberg, L. H. Dubois, N. J. Levinos, and L. Dhar, Phys. Rev. Lett. **64**, 2086 (1990).
[53] M. Bonn, C. Hess, and M. Wolf, J. Chem. Phys. **115**, 7725 (2001).
[54] W. G. Roeterdink, O. Berg, and M. Bonn, J. Chem. Phys. **121**, 10174 (2004).
[55] E. H. G. Backus, A. Eichler, A. W. Kleyn, and M. Bonn, Science **310**, 1790 (2005).
[56] K. Sekiguchi, S. Yamaguchi, and T. Tahara, J. Chem. Phys. **128**, 114715 (2008).
[57] L. Frydman, Annu. Rev. Phys. Chem. **52**, 463 (2001).
[58] S. Woutersen and P. Hamm, J. Phys.: Condens. Matter **14**, R1035 (2002).
[59] M. T. Zanni and R. M. Hochstrasser, Curr. Opin. Struct. Biol. **11**, 516 (2001).
[60] M. L. Cowan, B. D. Bruner, N. Huse, J. R. Dwyer, B. Chugh, E. T. J. Nibbering, T. Elsaesser, and R. J. D. Miller, Nature (London) **434**, 199 (2005).
[61] J. D. Eaves, J. J. Loparo, C. J. Fecko, S. T. Roberts, A. Tokmakoff, and P. L. Geissler, Proc. Natl. Acad. Sci. U.S.A. **102**, 13019 (2005).
[62] J. R. Zheng, K. Kwak, J. Asbury, X. Chen, I. R. Piletic, and M. D. Fayer, Science **309**, 1338 (2005).
[63] C. Kolano, J. Helbing, M. Kozinski, W. Sander, and P. Hamm, Nature (London) **444**, 469 (2006).
[64] J. Bredenbeck, J. Helbing, K. Nienhaus, G. U. Nienhaus, and P. Hamm, Proc. Natl. Acad. Sci. U.S.A. **104**, 14243 (2007).
[65] J. Bredenbeck, A. Ghosh, M. Smits, and M. Bonn, J. Am. Chem. Soc. **130**, 2152 (2008).
[66] M. Smits, A. Ghosh, M. Sterrer, M. Muller, and M. Bonn, Phys. Rev. Lett. **98**, 098302 (2007).
[67] A. Ghosh, M. Smits, J. Bredenbeck, and M. Bonn, J. Am. Chem. Soc. **129**, 9608 (2007).
[68] U. Emmerichs, S. Woutersen, and H. J. Bakker, J. Opt. Soc. Am. B **14**, 1480 (1997).
[69] M. Smits, A. Ghosh, J. Bredenbeck, S. Yamamoto, M. Muller, and M. Bonn, New J. Phys. **9**, 390 (2007).
[70] M. Bonn, C. Hess, J. H. Miners, T. F. Heinz, H. J. Bakker, and M. Cho, Phys. Rev. Lett. **86**, 1566 (2001).